NANO LETTERS
Cite This: Nano Lett. XXXX, XXX, XXX−XXX
Letter
pubs.acs.org/NanoLett

Controlling Bi-Provoked Nanostructure Formation in GaAs/GaAsBi Core−Shell Nanowires

Teruyoshi Matsuda,[†] Kyohei Takada,[†] Kohsuke Yano,[†] Rikuo Tsutsumi,[†] Kohei Yoshikawa,[†] Satoshi Shimomura,[†] Yumiko Shimizu,[‡] Kazuki Nagashima,*[,§] Takeshi Yanagida,[§] and Fumitaro Ishikawa*[,†]

[†]Graduate School of Science and Engineering, Ehime University, 3 Bunkyo-cho, Matsuyama, Ehime 790-8577, Japan
[‡]Toray Research Center, 3-3-7 Sonoyama, Otsu, Shiga 520-8567, Japan
[§]Institute for Materials Chemistry and Engineering, Kyushu University, Fukuoka 816-8580, Japan

Supporting Information

ABSTRACT: We control the formation of Bi-induced nanostructures on the growth of GaAs/GaAsBi core−shell nanowires (NWs). Bi serves as not only a constituent but also a surfactant and nanowire growth catalyst. Thus, we paved a way to achieve unexplored III−V nanostructures employing the characteristic supersaturation of catalyst droplets, structural modifications induced by strain, and incorporation into the host GaAs matrix correlated with crystalline defects and orientations. When Ga is deficient during growth, Bi accumulates on the vertex of core GaAs NWs and serves as a nanowire growth catalyst for the branched structures to azimuthal <112>. We find a strong correlation between Bi accumulation and stacking faults. Furthermore, Bi is preferentially incorporated on the GaAs (112)B surface, leading to spatially selective Bi incorporation into a confined area that has a Bi concentration of over 7%. The obtained GaAs/GaAsBi/GaAs heterostructure with an interface defined by the crystalline twin defects in a zinc-blende structure can be potentially applied to a quantum confined structure. Our finding provides a rational design concept for the creation of GaAsBi based nanostructures and the control of Bi incorporation beyond the fundamental limit.

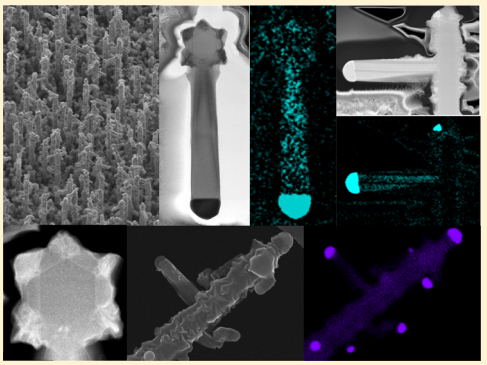

KEYWORDS: *Nanowire, nanostructure, heterostructure, GaAs, Bi, droplet*

Studying III−V semiconductor nanowires (NWs) has attracted much interest in recent decades due to their potential application in nanostructured electronic, photonic, and quantum devices.[1−3] The introduction of an epitaxial heterostructure facilitates control of the transport and electronic properties of such devices, showing the prospect for realizing integrated systems based on III−V compounds and Si with superior electronic and optical functions.[4−9] Branched or tree-like NWs offer an approach to increase structural complexity and enhance the resulting functions, which in turn enables the realization of higher-dimensionality structures, lateral connectivity, and interconnection between the NWs.[10−15] Such structures exhibit potential for applications in nanoscale quantum, photonic, electronic, energy conversion, and biological devices based on their complex configurations and large surface to volume ratio.[2,16−21] To synthesize branched NWs, conventionally, metallic catalyst nanoparticles, most commonly Au, are employed as the nucleation seeds for the growth of the branches.[10,13,22−24] Strain-driven vapor−liquid−solid (VLS) growth of branched III−V GaAs NWs using self-catalyst Ga droplets has been reported.[12,17] Optical devices based on III−V GaAs, such as lasers and optical amplifiers operating at the near-infrared regime, suffer from intrinsic losses related to Auger recombination. To circumvent this, the use of dilute bismide GaAsBi alloy has recently gained intensive attention, because the introduction of the Bi enlarges the splitting of the valence band energy levels between the heavy hole band and the spin−orbit band.[25−29] We recently obtained GaAs/GaAsBi heterostructure NWs on Si by using molecular beam epitaxy.[3,30,31] The GaAsBi NWs with a Bi concentration of 2% exhibit specific structural features, having a rough surface with corrugations,[30] which were probably induced by the large lattice mismatch and resulting strain accumulation between the GaAs and GaAsBi alloy.[32−36] Also, Bi acts as a surfactant to control the surface energy, thus provoking the synthesis of nanostructures.[37] Therefore, incorporating dilute bismide GaAsBi alloy into nanowires is a rational approach for developing high-performance optoelectronic nanodevices on account of its potential role in bandgap engineering and in the reduction of the intrinsic losses associated with Auger recombination in GaAs. However, the impact of Bi

Received: July 18, 2019
Revised: September 10, 2019
Published: September 17, 2019

DOI: 10.1021/acs.nanolett.9b02932
Nano Lett. XXXX, XXX, XXX−XXX

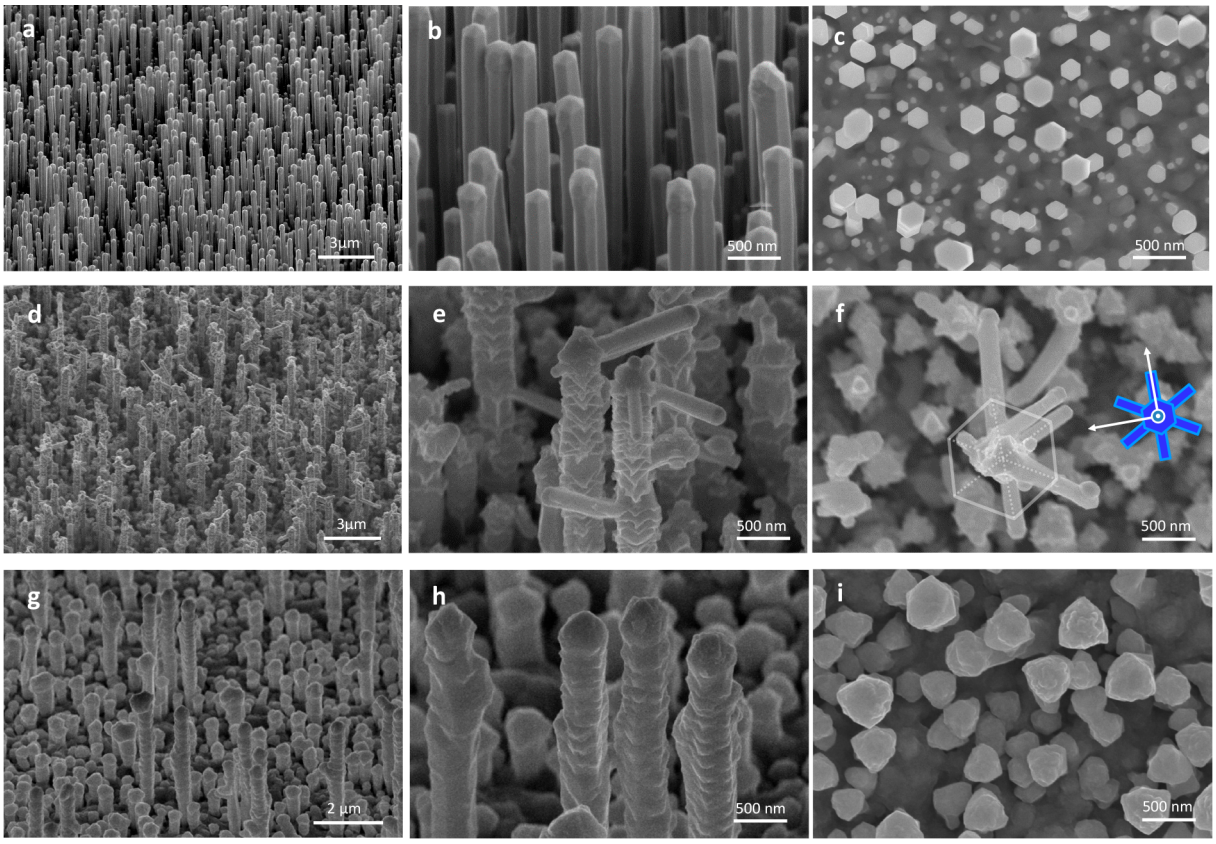

Figure 1. (a,b) 45°-tilted SEM images of GaAs/GaAsBi core−shell NWs grown at a Bi BEP of 6×10^{-8} mbar with the high-magnification image in (b) showing the tips of the NWs. (c) Planar SEM image. (d,e) 45°-tilted SEM images of GaAs/GaAsBi core−shell NWs grown at a Bi BEP of 5.4×10^{-7} mbar. The higher-magnification image in (e) shows the tips of the NWs, and the planar image in (f) shows the NWs' hexagonal guided structure. The blue overlay schematic illustrates the arrangement and orientation between the trunk and branches, where the branches grow from the apexes. (g) 45°-tilted SEM images of GaAs/GaAsBi/GaAs core−multishell NWs grown at a Bi BEP of 5.4×10^{-7} mbar at the GaAsBi shell and (h) a higher-magnification image showing the tip NW tips. (i) Planar SEM image of the NWs.

introduction on the GaAsBi alloy growth is far from being comprehensively understood. In this report, we investigate the features and growth mechanisms of GaAs/GaAsBi core−shell multilayered NWs on Si (111) substrates, focusing on the structural deformation induced by Bi.

The samples were grown by molecular beam epitaxy using constituent Ga-induced VLS growth on phosphorus-doped n-type Si (111) substrates.[38,39] The samples were heated to 580 °C under an As_4 beam equivalent pressure (BEP) of 1.0×10^{-5} mbar. The Ga supply was set to obtain a planar growth rate of 1.0 ML/s on GaAs (001) providing a group V As-rich growth condition. First, the GaAs core nanowires were grown for 15 min, and then, the growth was interrupted for 10 min, and the substrate temperature was reduced to 550 °C to crystallize the Ga catalyst. After crystallization of the catalyst, the lateral growth became dominant and was expected to yield core−shell-type NWs. We then supplied Ga flux for 15 min to form the GaAs shell and introduced growth interruption by further reducing the substrate temperature to 350 °C for the subsequent growth of GaAsBi. We then provided Ga and Bi flux nominally for 15 min to form the GaAsBi shell. Consequently, the NWs were expected to consist of a GaAs core surrounded by a GaAsBi shell layer. The widths of the GaAs core and GaAsBi shell were expected to be 100 and 80 nm, respectively. We first prepared two series of samples by varying the Bi flux during the growth of the GaAsBi shell. The BEP of As_4 was kept at 1.0×10^{-5} mbar throughout the growth, though one series of samples was grown with the Bi BEP adjusted to 6×10^{-8} mbar, and the other was grown with a Bi BEP of 5.4×10^{-7} mbar. All other growth conditions were identical among the samples. For the last sample, after the growth of the GaAs/GaAsBi core−shell structures (using the identical growth conditions as those of the sample grown at a Bi BEP of 5.4×10^{-7} mbar), without growth interruption, the outermost GaAs shell was grown for 15 min to form a GaAs/GaAsBi/GaAs core−multishell structure. After the structures were grown, the substrate temperature was reduced under As_4 pressure until it reached 300 °C. Subsequently, the As pressure was terminated, and the samples were removed after the substrate temperature cooled to below 100 °C. Notably, we simultaneously grew a GaAsBi thin film on GaAs (001) substrates placed on the growth substrate holder side by side. Based on X-ray diffraction characterization, the Bi concentration of the GaAsBi thin films grown at the Bi BEP of 6×10^{-8} mbar was found to be 1.3%.[31] The other thin film grown at the Bi BEP of 5.4×10^{-7} mbar had a Bi concentration of 4.5% with the existence of Bi droplets on the surface. However, our preliminary experiments on those NWs revealed that the NW samples contained 1.3% and about 2% Bi in the GaAsBi shell for the samples grown at the Bi BEPs of 6×10^{-8} and 5.4×10^{-7} mbar, respectively.[30,31] The Bi incorporation cannot monolithically be controlled, because that depends on several parameters, such as growth plane, temperature, and overpressure.[25−29] Hence, we investigate herein the incorporation

DOI: 10.1021/acs.nanolett.9b02932
Nano Lett. XXXX, XXX, XXX−XXX

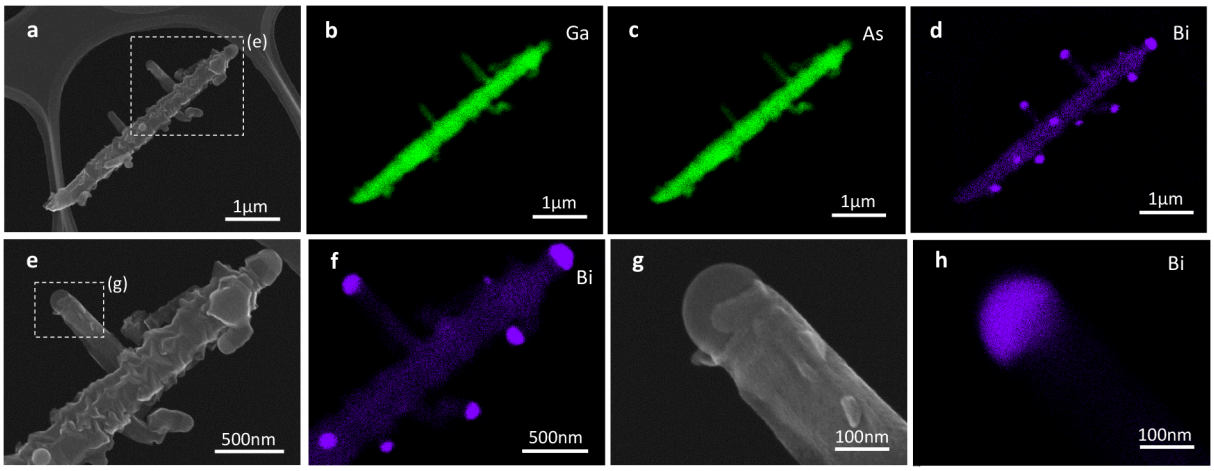

Figure 2. (a) SEM image and elemental (b–d) EDS mapping of Ga, As, and Bi, respectively, of a single branched GaAs/GaAsBi NW. The NW tip is located in the upper right of the image. (e) SEM image of the tip of the NW taken of the region delimited by a white square in (a), and (f) the corresponding elemental mapping of Bi. (g,h) High-magnification SEM image and Bi elemental mapping of the region indicated by the dashed rectangle shown in (e).

of Bi into NWs by focusing on the effect of growth conditions, microscopic characteristics, structure, and lattice plane. The NWs were investigated by scanning electron microscopy (SEM, JSM-7610F, JEOL, Japan) with energy dispersive X-ray spectroscopy (EDS). We also carried out cross-sectional scanning transmission electron microscopy (STEM) on axially and radially sliced single NW samples prepared by focused ion beam processing (Helios660, FEI, USA). STEM measurements were carried out on a TEM system (JEM-ARM200F Dual-X, JEOL, Japan) operating at 200 kV with EDS employing a 100 mm^2 silicon drift detector (JED-2300, JEOL). STEM images were obtained in both bright-field (BF) and high-angle annular dark-field (HAADF) modes, and fast Fourier transform (FFT) diffraction patterns were analyzed.

Figure 1(a,b) shows 45°-tilted SEM images of GaAs/GaAsBi core–shell NWs grown at a Bi BEP of 6×10^{-8} mbar. We observe the clear formation of aligned NWs growing approximately perpendicular from the substrate; the number density of the wires is 2×10^8 cm^{-2}. The NWs are typically 1–4 μm long, and the distribution of the wire diameter follows a Gaussian distribution with a peak at 250 nm and full width at half-maximum of 62 nm (shown in the Supporting Information).[38,39] The NWs have sharp-faceted sidewalls with a hexagonal cross section as shown in the planar SEM image presented in Figure 1(c).[30] The swelled NW tip results from the crystallization of the Ga catalyst during the growth interruption, which was introduced before the controlled shell layer formation.[38,39]

Figure 1(d,e) shows the 45°-tilted SEM image of the GaAs/GaAsBi core–shell NWs grown at a Bi BEP of 5.4×10^{-7} mbar, and Figure 1(f) shows a planar SEM image of the NWs. In contrast to the NWs grown at a Bi BEP of 6×10^{-8} mbar (Figures 1(a–c), those grown at a Bi BEP of 5.4×10^{-7} mbar (Figures 1(d–f)) exhibit a significantly different surface morphology. More specifically, the NWs have jagged surfaces and branches. The tips of the wire branches are round hemispheres and are associated with the catalyst that induced the branch formation.[12] In contrast to the rough surface on the primary trunk, the branch NWs exhibit a smooth surface. The trunk wire length varies between 1 and 6 μm, and the statistical distribution of the jagged NW trunk width is rather wide, i.e., 385 nm with a full width at half-maximum of 144 nm. Determining the length of the wire branch was difficult. However, owing to the smooth surface branches, the diameter could be estimated; the Gaussian distribution peak is at 192 nm, and the full width at half-maximum is 84 nm (shown in the Supporting Information).[38] The NWs shown in Figure 1(e) demonstrate branches that occasionally nucleated from the sharp-edged wire sidewall. As seen in the planar SEM image of the NWs in Figure 1(f), the growth of the branches is defined from the trunk crystal planes, resulting in the hexagonally radiated structure. The branches are oriented to <112> directions, which will be discussed further in the following discussion about the TEM investigation. The wires originate from the apexes, i.e., the vertices between the adjacent {110} side planes.[30,40] These results are different from commonly observed branches that protrude from azimuthal {111}-related planes as Zha et al. reported,[12] where the branch nucleation induced by the Ga droplet on the NW surface favors the trunk vertex due to stress release.

Figure 1(g,h) shows 45°-tilted SEM images of GaAs/GaAsBi/GaAs core–multishell NWs grown at a Bi BEP of 5.4×10^{-7} mbar. The planar SEM image of the NWs is shown in Figure 1(i), and the number density of the wires is 4×10^8 cm^{-2}. The NWs typically have a length of 1–5 μm, and the distribution of the wire diameter follows a Gaussian distribution with a peak at 389 nm and full width at half-maximum of 73 nm (shown in the Supporting Information). Due to the longer growth time of the shell layer, the NWs are thicker.[38,39] The NW surface and tip are undulated. Branches are not observed despite the growth until the middle GaAsBi layer being identical to the growth of the wires shown in Figure 1(d–f); however, here, the subsequent GaAs outermost shell growth was achieved by supplying Ga flux. Hence, comparing the morphologies provides key information about the branch formation. Notably, we have observed a similar feature with the characteristic surface morphology in the GaAs/GaAsBi/GaAs core–multishell NWs grown with mostly identical growth conditions except for thinner GaAsBi layer widths.[30] The analysis for these reproducible structural deformations of these NWs should provide the general understanding of the growth mechanism on this material system.

DOI: 10.1021/acs.nanolett.9b02932
Nano Lett. XXXX, XXX, XXX–XXX

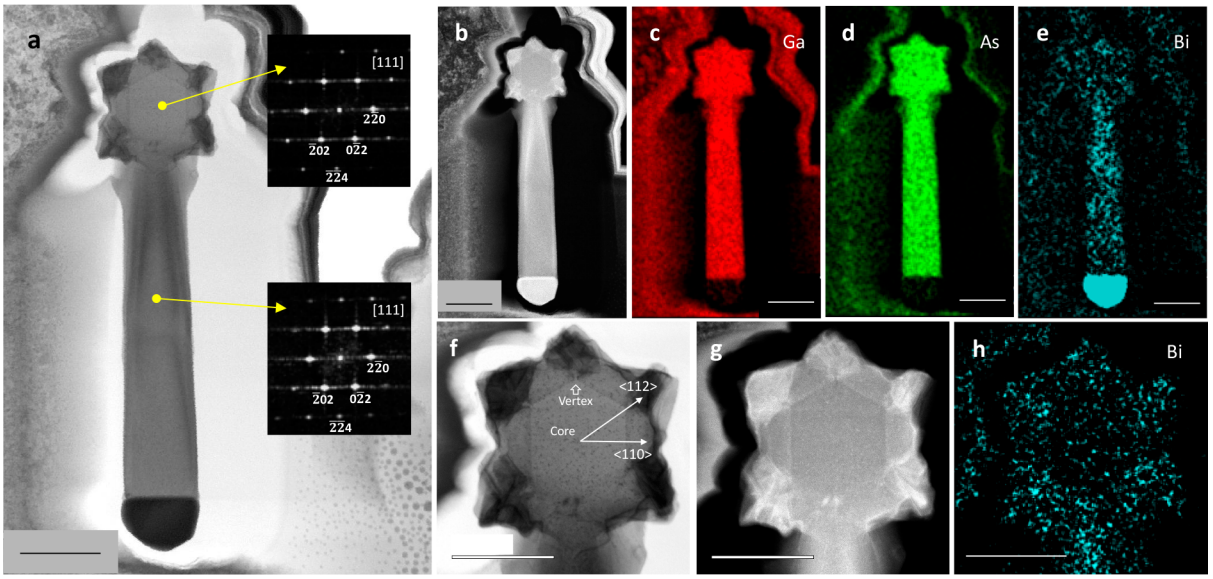

Figure 3. Axial cross-sectional STEM study of the branched GaAs/GaAsBi core−shell NW, observed from the [111] direction. (a) BF-STEM image with insets indicated in yellow showing FFT electron diffraction patterns obtained at the trunk and middle of the branch. (b−e) HAADF-STEM and EDS elemental mapping of Ga, As, and Bi, respectively. (f) High-magnification BF-STEM and (g) HAADF-STEM images and (h) EDS elemental mapping of Bi of the cross section of the trunk in (f,g). The scale bars are 200 nm.

Figure 2(a−h) presents SEM images and EDS maps of a typical NW with branches, where the GaAs/GaAsBi core−shell NWs were grown at a Bi BEP of 5.4×10^{-7} mbar. As seen in Figure 2(b−d), the primary trunk shows strong Ga and As content, and the Bi intensity is weaker. The trunk is a NW consisting of GaAsBi, which agrees well with the expected Bi concentration of 2−3% from preliminary studies.[30] The wire branches similarly exhibit high Ga and As content and low Bi content. Hence, the results suggest that the wire branches consist of GaAsBi. Considering the smooth surface of the branches in contrast to the jagged surface of the trunk, the strain of the trunk and branches should be significantly different. The hemispherical tip morphology is observed for both the primary trunk and the branches. As clearly seen in the Bi elemental mapping images in Figure 2(d,f,h), the hemisphere originates from Bi. It is noteworthy that no Ga is observed at the tip, as seen in Figure 2(b). In a previous report by Zha et al, a Ga droplet acts as the catalyst for the VLS growth of the branches.[12] Considering that the Bi BEP for the NWs having jagged surfaces (5.4×10^{-7} mbar) is much larger than that for the NWs with smooth surface morphology (as shown in Figure 1(a,b), 6×10^{-8} mbar), similar to the expected Bi concentration (1.3% for the smooth surface NWs and 2−3% for the NWs having jagged surfaces),[30,31] more than 70% of the irradiated Bi is not introduced into the GaAsBi layer, and thus, excess metallic Bi is produced on the growth front. Probably, the excess Bi forms droplets on the surface as seen on the GaAs (001) substrate, which was simultaneously mounted at the growth of the branched NW sample (shown in the Supporting Information). The droplets formed on the smooth GaAs (001) thin film probably have a larger diffusion length than that on the Si (111) substrate with NWs, where the coalescence of the droplets would be enhanced. Thus, the droplets on the GaAs (001) film should have a larger diameter and smaller density compared to those on the Si (111) substrate having NWs. Further, the cooling procedure under As overpressure after the growth could change the feature of the droplets on the surface. Nevertheless, the surface droplets on GaAs (001) substrate grown under identical conditions provides valuable information about the growth front of the NWs. The droplets should mainly comprise Bi. Additionally, the existence of Bi droplets very possibly promotes the formation of the NW branches. Further, the existence of additional Ga and As overpressure with the Bi droplets induces characteristic supersaturation, resulting in the formation of a needle-like nanocrystal as seen in the Supporting Information. Such a phenomenon might be related to the jagged surface observed in the branched NWs shown in Figures 1(d−f).

Figure 3(a−h) shows axial cross-sectional BF-STEM, HAADF-STEM, EDS images, and FFT diffraction patterns of the branched GaAs/GaAsBi core−shell NW. The measurement was carried out from the [111] direction. Figure 3(a) shows the BF-STEM image of the branched NW. The branch nucleates from the trunk of the NW. The FFT electron diffraction pattern shows an identical crystal orientation between the trunk and the middle of the branch. Therefore, it can be concluded that the wire is grown epitaxially from the trunk. Figure 3(b−e) shows an HAADF-STEM image and EDS elemental mappings for Ga, As, and Bi, respectively. The NW mainly consists of GaAs and also includes a small amount of Bi for both the trunk and branch. As also seen in Figure 2, there is a Bi cluster at the tip of the NW. The HAADF image provides information about the elemental distribution based on its Z-contrast image, where elements of larger atomic number exhibit brighter contrast. The bright contrast in the HAADF image of Figure 3(b) corresponds to the Bi intensity in Figure 3(e). Figure 3(f−h) shows higher magnification BF-STEM and HAADF-STEM images and EDS elemental mapping for Bi for the trunk, individually. Inside the NW trunk, a GaAs core showing hexagonal vertexes is observed. Considering the FFT diffraction patterns shown in Figure 3(a), the vertices are directed to <112> between the adjacent {110} side planes. The lattice distances obtained from the FFT patterns are 0.194 and 0.201 nm for $(2\bar{2}0)$ and $(0\bar{2}2)$ diffraction, respectively, at the center of the wire trunk, and these are similar to the standard GaAs lattice constants. On the other hand, the same lattice

DOI: 10.1021/acs.nanolett.9b02932
Nano Lett. XXXX, XXX, XXX−XXX

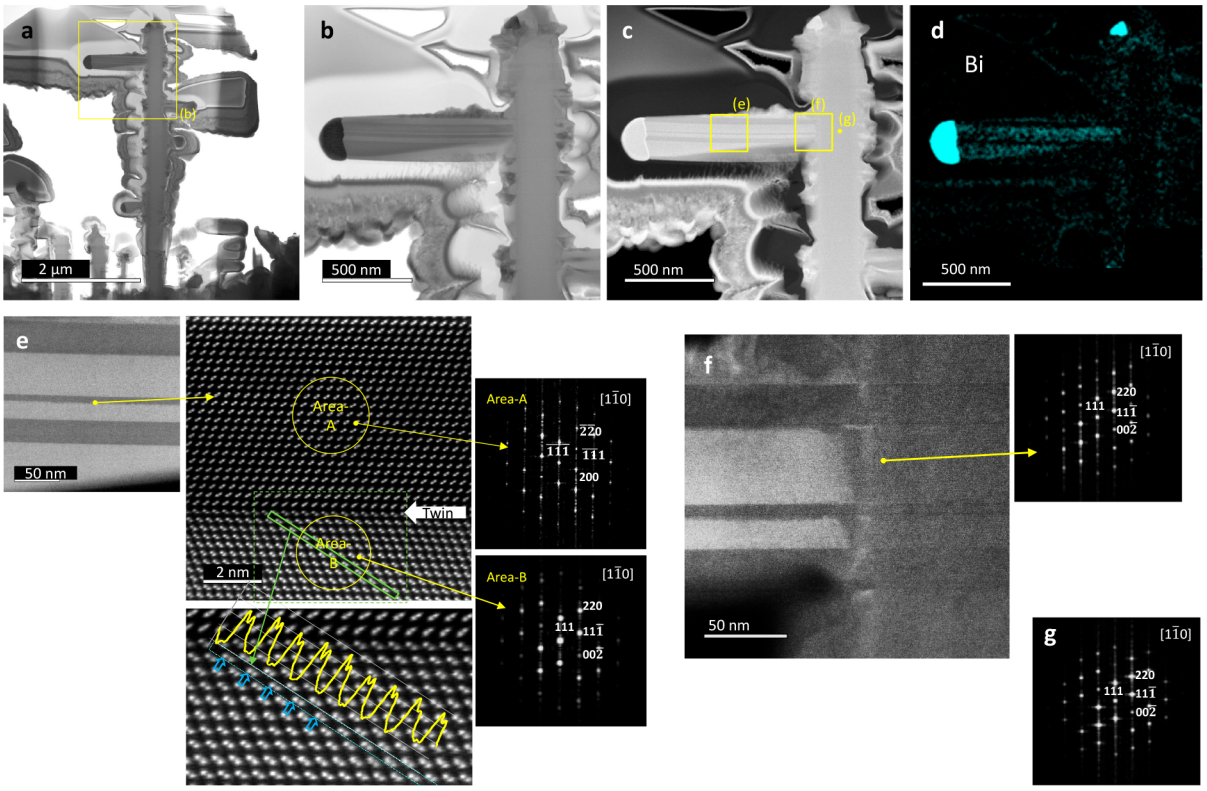

Figure 4. (a) Cross-sectional BF-STEM image of a branched wire growing out of the substrate and (b) a higher-magnification image of the area around the trunk tip delimited by the yellow rectangle in (a). (c) HAADF-STEM image and (d) EDS elemental mapping of Bi for the areas delimited by the yellow square in (a) for the branched GaAs/GaAsBi core−shell nanowire, as observed from the [110] direction. (e) High-magnification HAADF-STEM image taken of the area in (c) delimited by the labeled yellow square. The filtered HAADF image obtained at the interface between the bright and dark contrast regions as indicated and its high-resolution image for areas A and B, where brighter atoms corresponding to group V sites are indicated by yellow arrows, and FFT patterns obtained for areas A and B are indicated by yellow circles. (f) High-magnification HAADF-STEM image of the root of the branch taken of the area in (c) delimited by the labeled yellow square, and FFT pattern obtained for the spot indicated by the yellow arrow. (g) FFT pattern obtained for the spot at the middle of the trunk as indicated in (c) by a labeled yellow dot.

constants measured in the middle of the branch are 0.213 and 0.204 nm for (2$\bar{2}$0) and (0$\bar{2}$2) diffraction, respectively. That indicates the GaAsBi at the middle of the wire branch is deformed by the introduction of Bi, which has a larger lattice constant than that of the GaAs in the NW core at the middle of the wire trunk. The branch is directed to <112> and originates from a vertex of the GaAs core.[30,40] The structure of the outer shell has a characteristic hexagonal-star structure that is probably induced by the presence of Bi at the vertex of the outermost shell; large density stacking faults are observed by the dark contrast in Figure 3(f) and are likely induced by the accumulation of Bi, which is confirmed by the bright contrast in Figure 3(g) and the Bi elemental mapping shown in Figure 3(h). As seen from the dark contrast of the BF-STEM image in Figure 3(f), there are many stacking faults at the outer shell of the vertexes where there are no branches. On the other hand, the vertex with a branch protruding from it exhibits much smaller stacking faults, which suggests that the branch formation suppresses the formation of crystalline defects. By comparing the BF-STEM and HAADF-STEM images and Bi elemental distribution from Figure 3(f−h), the locations correspond to stacking faults, the bright contrast of the HAADF image, and the location of Bi. These results suggest that there is an interaction between the crystalline defects and the presence of Bi.

Figure 4(a−f) shows a series of cross-sectional STEM images and EDS investigations of a branched NW growing from the substrate (hereafter, known as radial cross-sectional STEM). As seen in the figures, the branch protrudes perpendicular to the NW trunk, as expected from its direction (toward the <112> orientation). The bright contrast in the HAADF image in Figure 4(c) clearly corresponds to the strong intensity of Bi in Figure 4(d). Specifically, the horizontally striped switching of the HAADF image contrast in Figure 4(c) can be observed within the branch, which also agrees with the BF-STEM image in Figure 4(b) and the EDS Bi intensity in Figure 4(d). It is noteworthy that the quantified Bi concentration based on EDS is 0% in the core of the trunk. On the other hand, 7% Bi within the group V elements is observed at the biaccumulated area in the middle of the branches (EDS investigation is shown in Supporting Information). Considering the growth conditions at the substrate temperature of 350 °C under group V As-rich conditions, the amount is much larger than the reported values for the thin films.[41] The tip of the NW contains about 5% of Ga and As, which make it impossible to determine the tip metal crystal to be mainly metallic Bi crystal. The striped area in the branch shown in Figure 4(e) is also interesting; at the interface of the contrast switching, there is a twin defect of the zinc-blende GaAs structure that is clearly seen in the filtered atomic HAADF image. Notably, the NW studied dominantly

DOI: 10.1021/acs.nanolett.9b02932
Nano Lett. XXXX, XXX, XXX−XXX

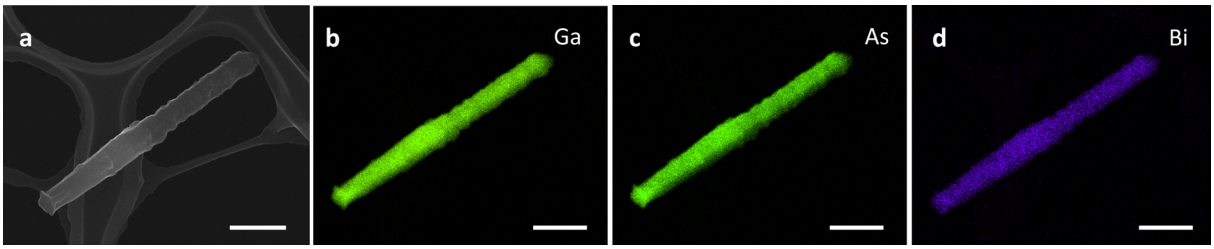

Figure 5. (a) SEM image and (b–d) elemental EDS mapping for Ga, As, and Bi for a single GaAs/GaAsBi/GaAs core–multishell NW grown at a Bi BEP = 5.4 × 10^{-7} mbar. The NW tip is located in the upper right of the image. The scale bar is 1 μm.

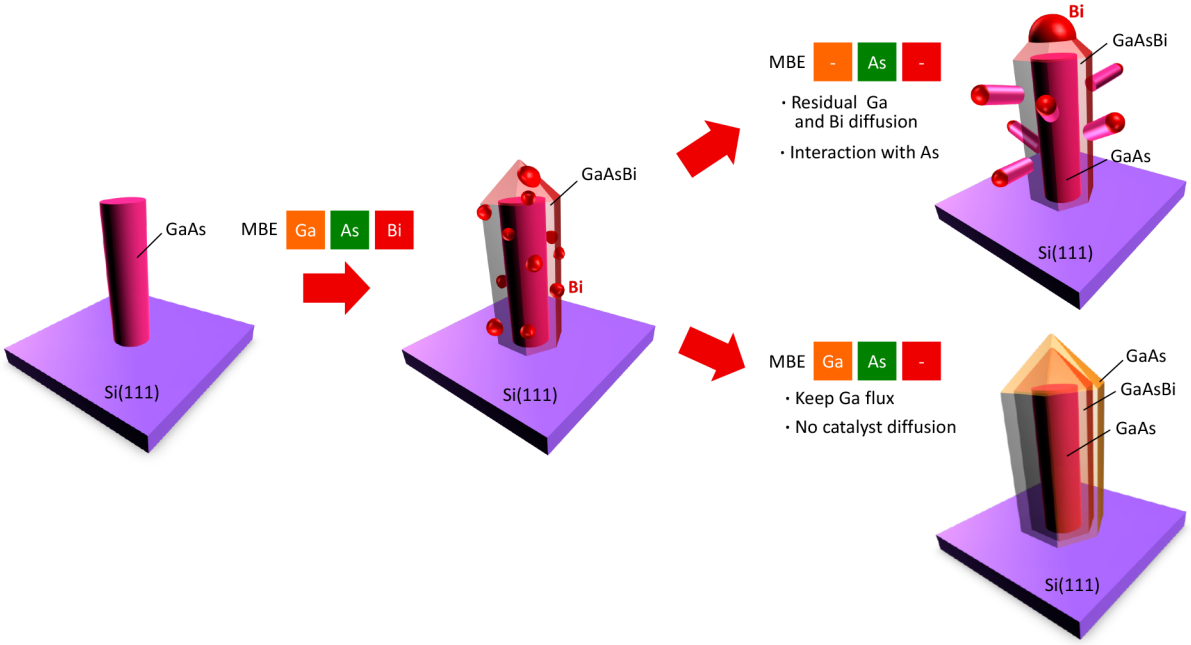

Figure 6. Schematic of the growth mechanism with the residual Bi on a nanowire growth front.

comprised a zinc-blende structure with numbers of twins. Conversely, the existence of the wurtzite phase was negligible throughout the NW. In particular, as seen in Figure 4(e), the lower part, labeled as area B, has a brighter contrast corresponding to the Bi-rich area of Figure 4(d). From the high-resolution HAADF image of area B (see lower center panel of Figure 4(e)), we can resolve the present atoms by the intensity of observed atoms. As seen in the intensity profile, the upper left atoms of the paired atoms in the image are more intense than the lower left side atoms and thus correspond to the group V As or Bi. On the other hand, such a clear difference in the intensity between the pair elements could not be observed in area A, suggesting that these may be constituent Ga and As, which are close in atomic number, with a trace amount of Bi in the group V site in the area (shown in the Supporting Information). Hence, the observed higher Bi composition in area B would be caused by the surface configuration at the growth front, where As-rich (112)B surfaces having higher surface energy are exposed, promoting the introduction of Bi into the layer.[42−44] The diffraction pattern in area A provides the lattice distance 0.283 nm for $(\bar{1}11)$ and 0.259 nm for (200). On the other hand, for area B, the distance is 0.288 nm for (111) and 0.267 nm for $(00\bar{2})$ diffraction. Considering the standard lattice distances for GaAs, 0.326 nm for (111) and 0.283 nm for (200), the measured values are smaller for both the orientations in contrast to the results obtained for the axial cross-sectional investigation shown in Figure 3(a), which are longer (expanded) than the standard values. Hence, the lattice is three-dimensionally distorted in the branch, namely, it is extended in the axial/horizontal direction, but it is shrunken especially for the {111} planes of the radial/vertical directions. The observed large strain, larger than 5% at its lowest, induces the observed structural deformations that have also been reported to form surface undulations in GaAsBi thin film[34] and NWs.[30] In addition, the surface roughening exposes various crystal orientations on the branch surface. Therefore, the (112) oriented surface possibly acts as the preferential site for the nucleation of an additional nanocrystal, inducing the formation of the observed branches.[45] Figure 4(f) shows the high-resolution HAADF-STEM image of the area at the root of the branch in the shell layers of the trunk. From the contrast observed in the image, the twin defect interface is penetrated and preserved from the trunk to the branch. The apparent contrast switch occurs at the branch. Consequently, the twin defect is preserved at the epitaxial nucleation of the wire branch. The growth of the GaAs or GaAsBi occurs during the growth with the Bi catalyst at the tip of the nanowire. There, Bi dominantly incorporates for a preferable crystal orientation that is switched by the twin, which is propagated from the GaAs trunk core. In particular, the heterointerface between GaAs and GaAsBi was defined by crystalline twin defects,

DOI: 10.1021/acs.nanolett.9b02932
Nano Lett. XXXX, XXX, XXX−XXX

which are realized by the characteristic growth mechanism related to Bi in this material system.[25,29] Considering the smaller band gap energy for the GaAsBi alloy, the structure will potentially be assigned as a GaAs/GaAsBi/GaAs quantum confined structure. At the root area, the diffraction pattern provides lattice constants of 0.315 nm for (111) and 0.278 nm for $(00\bar{2})$, which are more than 10% larger than the values at both areas A and B observed in the branch (Figure 4(e)). The core area also exhibits a lattice constant of 0.300 nm for (111), as obtained from the diffraction pattern in Figure 4(g). The observed lattice distances are close to that of GaAs. Hence, the lattice shrinkage is observed only in the wire branch, which would be the specific lattice deformation induced by the branching with Bi.

Figure 5(a–d) shows SEM and EDS images for a GaAs/GaAsBi/GaAs core–multishell NW grown at a Bi BEP of 5.4×10^{-7} mbar at the GaAsBi shell. The growth was carried out under growth conditions identical with those for the branched NWs shown in Figures 2–4 except for the addition of Ga for 15 min after growth under the As flux. The wire does not show branches. The wire surface is not flat but corrugated, which was probably induced by the introduction of Bi at the GaAsBi shell. As seen in Figure 5(d), Bi is present throughout the NW. Notably, the feature of this NW is very similar to our previous report of a GaAs/GaAsBi/GaAs core–multishell NW grown at mostly identical conditions except for a thinner GaAsBi shell.[30] The reproductivity of this characteristic corrugated surface should be a certification of the general trend of bimodulated structural deformations in this material system.

Figure 6 illustrates the formation mechanism of branched NWs based on the results of growing NWs having a GaAsBi shell grown at a Bi BEP of 5.4×10^{-7} mbar. Here, after the growth of the GaAsBi shell for the trunk, we maintain the As overpressure for a certain period, which allows As to sufficiently interact with the residual Ga and Bi on the growth front. Even when the Ga BEP is turned off at the end of the GaAsBi shell growth on the trunk, residual Bi is present on the surface, which largely diffuses over the surface. Considering the presence of the Bi hemisphere on the tip of the trunk and branches, Ga would have existed in the metallic droplet for the VLS formation of branches with Bi, which acts as a catalyst. The branch formation would be driven by this process, where the residual Ga and Bi on the surface eventually crystallize with the atmospheric As. However, when we supply Ga after the growth of GaAsBi, the Ga interacts with As and crystallizes, forming the outermost GaAs shell layer. This result indicates that the additional Ga after the growth of the GaAsBi shell layer does not support droplet formation and branching. Consequently, we conclude that the branch formation is induced by the residual Bi that forms a Bi droplet and acts as the catalyst for the branch formation.

In summary, to control the formation of complex structures in GaAsBi NWs by introducing Bi, we investigated the effect of Bi on the growth of GaAs/GaAsBi core–shell NWs. When we supply more Bi, which provides excess Bi at the growth front, the Bi induces dramatic structural modifications to the NWs. The introduction of Bi into the GaAs matrix induces large strain and three-dimensional distortions of the lattice structure. The strain also results in the formation of stacking faults and undulations of the NW surface. The NWs then exhibit a hexagonal-star cross-sectional structure. The Bi droplet on the undulated NW surface acts as the catalyst of VLS growth of the GaAsBi NW branches to the <112> directions, corresponding to a vertex of the NW core. The introduction of Bi into the GaAs matrix is promoted on the (112)B surface; regions of different Bi compositions are present, between which twin defects are found. The obtained GaAs/GaAsBi/GaAs heterostructure with an interface defined by the crystalline twin defects in a zinc-blende structure can be potentially applied to a quantum confined structure. Based on the understandings obtained in this study, we can control the deformation, distortion, and branching of GaAsBi NWs by introducing Bi, which results in complex high-dimensional configurations that may enhance the functionality of the structures.

■ ASSOCIATED CONTENT

Supporting Information

The Supporting Information is available free of charge on the ACS Publications website at DOI: 10.1021/acs.nanolett.9b02932.

Density, length, and diameters of the nanowires; Bi droplets on the GaAs (001) substrate simultaneously mounted with the branched nanowire sample at the growth; sample preparation for the cross-sectional STEM investigations on branched GaAs/GaAsBi core–shell nanowires; additional information for cross-sectional STEM investigations of branched GaAs/GaAsBi core–shell nanowires (PDF)

■ AUTHOR INFORMATION

Corresponding Authors

*E-mail: kazu-n@cm.kyushu-u.ac.jp. (K.N.)
*E-mail: ishikawa.fumitaro.zc@ehime-u.ac.jp. (F.I.)

ORCID

Kazuki Nagashima: 0000-0003-0180-816X
Takeshi Yanagida: 0000-0003-4837-5701
Fumitaro Ishikawa: 0000-0002-5632-056X

Notes

The authors declare no competing financial interest.

■ ACKNOWLEDGMENTS

This study was partly supported by the funding support from KAKENHI (No. 16H05970 and 19H00855) from the Japan Society of Promotion of Science. K.N. was supported by the MEXT Project of "Integrated Research Consortium on Chemical Sciences".

■ REFERENCES

(1) Gudiksen, M. S.; Lauhon, L. J.; Wang, J.; Smith, D. C.; Lieber, C. M. Growth of nanowire superlattice structures for nanoscale photonics and electronics. *Nature* **2002**, *415*, 617–620.

(2) Zhang, H.; Liu, C.-X.; Gazibegovic, S.; Xu, D.; Logan, J. A.; Wang, G.; van Loo, N.; Bommer, J. D. S.; de Moor, M. W. A.; Car, D.; Op het Veld, R. L. M.; van Veldhoven, P. J.; Koelling, S.; Verheijen, M. A.; Pendharkar, M.; Pennachio, D. J.; Shojaei, B.; Lee, J. S.; Palmstrøm, C. J.; Bakkers, E. P. A. M.; Das Sarma, S.; Kouwenhoven, L. P. Quantized Majorana conductance. *Nature* **2018**, *556*, 74–79.

(3) *Novel Compound Semiconductor Nanowires: Materials, Devices, and Applications*; Ishikawa, F., Buyanova, I. A., Eds.; Pan Stanford Publishing: Singapore, 2017.

(4) Mårtensson, T.; Svensson, C. P. T.; Wacaser, B. A.; Larsson, M. W.; Seifert, W.; Deppert, K.; Gustafsson, A.; Wallenberg, L. R.; Samuelson, L. Epitaxial III– V nanowires on silicon. *Nano Lett.* **2004**, *4*, 1987–1990.

DOI: 10.1021/acs.nanolett.9b02932
Nano Lett. XXXX, XXX, XXX–XXX

(5) Li, Q.; Ng, K. W.; Lau, K. M. Growing antiphase-domain-free GaAs thin films out of highly ordered planar nanowire arrays on exact (001) silicon. *Appl. Phys. Lett.* **2015**, *106*, No. 072105.
(6) Tomioka, K.; Yoshimura, M.; Fukui, T. A III−V nanowire channel on silicon for high-performance vertical transistors. *Nature* **2012**, *488*, 189−192.
(7) Björk, M. T.; Thelander, C.; Hansen, A. E.; Jensen, L. E.; Larsson, M. W.; Wallenberg, L. R.; Samuelson, L. Few-electron quantum dots in nanowires. *Nano Lett.* **2004**, *4*, 1621−1625.
(8) Tang, J.; Huo, Z.; Brittman, S.; Gao, H.; Yang, P. Solution-processed core−shell nanowires for efficient photovoltaic cells. *Nat. Nanotechnol.* **2011**, *6*, 568−572.
(9) Songmuang, R.; Giang, L. T. T.; Bleuse, J.; Den Hertog, M.; Niquet, Y. M.; Dang, L. S.; Mariette, H. Determination of the optimal shell thickness for self-catalyzed GaAs/AlGaAs core−shell nanowires on silicon. *Nano Lett.* **2016**, *16*, 3426−3433.
(10) Dick, K. A.; Deppert, K.; Larsson, M. W.; Martensson, T.; Seifert, W.; Wallenberg, L. R.; Samuelson, L. Synthesis of branched nanotrees by controlled seeding of multiple branching events. *Nat. Mater.* **2004**, *3*, 380−384.
(11) Jiang, X.; Tian, B.; Xiang, J.; Qian, F.; Zheng, G.; Wang, H.; Mai, L.; Lieber, C. M. Rational growth of branched nanowire heterostructures with synthetically encoded properties and function. *Proc. Natl. Acad. Sci. U. S. A.* **2011**, *108*, 12212−12216.
(12) Zha, G.; Li, M.; Yu, Y.; Wang, L.; Xu, J.; Shang, X.; Ni, H.; Niu, Z. Strain-driven synthesis of self-catalyzed branched GaAs nanowires. *Appl. Phys. Lett.* **2013**, *102*, 163115.
(13) Wang, D.; Qian, F.; Yang, C.; Zhong, Z. A.; Lieber, C. M. Rational growth of branched and hyperbranched nanowire structures. *Nano Lett.* **2004**, *4*, 871−874.
(14) Dick, K. A.; Deppert, K.; Karlsson, L. S.; Seifert, W.; Wallenberg, L. R.; Samuelson, L. Position-controlled interconnected InAs nanowire networks. *Nano Lett.* **2006**, *6*, 2842−2847.
(15) Lugstein, A.; Andrews, A. M.; Steinmair, M.; Hyun, Y.-J.; Bertagnolli, E.; Weil, M.; Pongratz, P.; Schramböck, M.; Roch, T.; Strasser, G. Growth of branched single-crystalline GaAs whiskers on Si nanowire trunks. *Nanotechnology* **2007**, *18*, 355306.
(16) Gazibegovic, S.; Car, D.; Zhang, H.; Balk, S. C.; Logan, J. A.; de Moor, M. W. A.; Cassidy, M. C.; Schmits, R.; Xu, D.; Wang, G.; Krogstrup, P.; Op het Veld, R. L. M.; Zuo, K.; Vos, Y.; Shen, J.; Bouman, D.; Shojaei, B.; Pennachio, D.; Lee, J. S.; van Veldhoven, P. J.; Koelling, S.; Verheijen, M. A.; Kouwenhoven, L. P.; Palmstrøm, C. J.; Bakkers, E. P. A. M. Epitaxy of advanced nanowire quantum devices. *Nature* **2017**, *548*, 434−438.
(17) Yu, Y.; Zha, G.-W.; Shang, X.-J.; Yang, S.; Sun, B.-Q.; Ni, H.-Q.; Niu, Z.-C. Self-assembled semiconductor quantum dots decorating the facets of GaAs nanowire for single-photon emission. *Nat. Sci. Rev.* **2017**, *4*, 196−209.
(18) Yu, Y.; Li, M.-F.; He, J.-F.; He, Y.-M.; Wei, Y.-J.; He, Y.; Zha, G.-W.; Shang, X.-J.; Wang, J.; Wang, L.-J.; Wang, G.-W.; Ni, H.-Q.; Lu, C.-Y.; Niu, Z.-C. Single InAs quantum dot grown at the junction of branched gold-free GaAs nanowire. *Nano Lett.* **2013**, *13*, 1399−1404.
(19) Rahong, S.; Yasui, T.; Yanagida, T.; Nagashima, K.; Kanai, M.; Klamchuen, A.; Meng, G.; He, Y.; Zhuge, F.; Kaji, N.; Kawai, T.; Baba, Y. Ultrafast and wide range analysis of DNA molecules using rigid network structure of solid nanowires. *Sci. Rep.* **2015**, *4*, 5252.
(20) Sun, K.; Jing, Y.; Li, C.; Zhang, X.; Aguinaldo, R.; Kargar, A.; Madsen, K.; Banu, K.; Zhou, Y.; Bando, Y.; Liu, Z.; Wang, D. 3D branched nanowire heterojunction photoelectrodes for high-efficiency solar water splitting and H_2 generation. *Nanoscale* **2012**, *4*, 1515−1521.
(21) Bierman, M. J.; Jin, S. Potential applications of hierarchical branching nanowires in solar energy conversion. *Energy Environ. Sci.* **2009**, *2*, 1050−1059.
(22) Paladugu, M.; Zou, J.; Auchterlonie, G. J.; Guo, Y. N.; Kim, Y.; Joyce, H. J.; Gao, Q.; Tan, H. H.; Jagadish, C. Evolution of InAs branches in InAs/GaAs nanowire heterostructures. *Appl. Phys. Lett.* **2007**, *91*, 133115.
(23) Dick, K. A.; Geretovszky, Z.; Mikkelsen, A.; Karlsson, L. S.; Lundgren, E.; Malm, J.-O.; Andersen, J. N.; Samuelson, L.; Seifert, W.; Wacaser, B. A.; Deppert, K. Improving InAs nanotree growth with composition-controlled Au−In nanoparticles. *Nanotechnology* **2006**, *17*, 1344.
(24) Jung, Y.; Ko, D.-K.; Agarwal, A. R. Synthesis and structural characterization of single-crystalline branched nanowire heterostructures. *Nano Lett.* **2007**, *7*, 264−268.
(25) Yoshimoto, M.; Murata, S.; Chayahara, A.; Horino, Y.; Saraie, J.; Oe, K. Metastable GaAsBi Alloy Grown by Molecular Beam Epitaxy. *Jpn. J. Appl. Phys.* **2003**, *42*, L1235.
(26) Tixier, S.; Adamcyk, M.; Tiedje, T.; Francoeur, S.; Mascarenhas, A.; Wei, P.; Schiettekatte, F. Molecular beam epitaxy growth of $GaAs_{1-x}Bi_x$. *Appl. Phys. Lett.* **2003**, *82*, 2245.
(27) Puustinen, J.; Wu, M.; Luna, E.; Schramm, A.; Laukkanen, P.; Laitinen, M.; Sajavaara, T.; Guina, M. Variation of lattice constant and cluster formation in GaAsBi. *J. Appl. Phys.* **2013**, *114*, 243504.
(28) Richards, R. D.; Mellor, A.; Harun, F.; Cheong, J. S.; Hylton, N. P.; Wilson, T.; Thomas, T.; Roberts, J. S.; Ekins-Daukes, N. J.; David, J. P. R. Photovoltaic characterisation of GaAsBi/GaAs multiple quantum well devices. *Solar Energy Mater. Solar Cells* **2017**, *172*, 238−243.
(29) Wang, L.; Zhang, L.; Yue, L.; Liang, D.; Chen, X.; Li, Y.; Lu, P.; Shao, J.; Wang, S. Novel dilute bismide, epitaxy, physical properties and device application. *Crystals* **2017**, *7*, 63.
(30) Ishikawa, F.; Akamatsu, Y.; Watanabe, K.; Uesugi, F.; Asahina, S.; Jahn, U.; Shimomura, S. Metamorphic GaAs/GaAsBi Heterostructured Nanowires. *Nano Lett.* **2015**, *15*, 7265−7272.
(31) Matsuda, T.; Takada, K.; Yano, K.; Shimomura, S.; Ishikawa, F. Strain deformation in GaAs/GaAsBi core-shell nanowire heterostructures. *J. Appl. Phys.* **2019**, *125*, 194301.
(32) Tixier, S.; Adamcyk, M.; Tiedje, T.; Francoeur, S.; Mascarenhas, A.; Wei, P.; Schiettekatte, F. Molecular beam epitaxy growth of $GaAs_{1-x}Bi_x$. *Appl. Phys. Lett.* **2003**, *82*, 2245.
(33) Hwang, J.; Phillips, J. D. Band structure of strain-balanced GaAsBi/GaAsN superlattices on GaAs. *Phys. Rev. B: Condens. Matter Mater. Phys.* **2011**, *83*, 195327.
(34) Bastiman, F.; Mohmad, A. R. B.; Ng, J. S.; David, J. P. R.; Sweeney, S. J. Non-stoichiometric GaAsBi/GaAs (100) molecular beam epitaxy growth. *J. Cryst. Growth* **2012**, *338*, 57−61.
(35) Fluegel, B.; Francoeur, S.; Mascarenhas, A.; Tixier, S.; Young, E. C.; Tiedje, T. Giant Spin-Orbit Bowing in $GaAs_{1-x}Bi_x$. *Phys. Rev. Lett.* **2006**, *97*, No. 067205.
(36) Kudrawiec, R.; Kopaczek, J.; Polak, M. P.; Scharoch, P.; Gladysiewicz, M.; Misiewicz, J.; Richards, R. D.; Bastiman, F.; David, J. P. R. Experimental and theoretical studies of band gap alignment in $GaAs_{1-x}Bi_x$/GaAs quantum wells. *J. Appl. Phys.* **2014**, *116*, 233508.
(37) Lewis, R. B.; Corfdir, P.; Herranz, J.; KüPers, H.; Jahn, U.; Brandt, O.; Geelhaar, L. Self-assembly of InAs nanostructures on the sidewalls of GaAs nanowires directed by a Bi surfactant. *Nano Lett.* **2017**, *17*, 4255−4260.
(38) Araki, Y.; Yamaguchi, M.; Ishikawa, F. Growth of dilute nitride GaAsN/GaAs heterostructure nanowires on Si substrates. *Nanotechnology* **2013**, *24*, No. 065601.
(39) Ahn, N.; Araki, Y.; Kondow, M.; Yamaguchi, M.; Ishikawa, F. Effects of growth interruption, As and Ga fluxes, and nitrogen plasma irradiation on the molecular beam epitaxial growth of GaAs/GaAsN core−shell nanowires on Si (111). *Jpn. J. Appl. Phys.* **2014**, *53*, No. 065001.
(40) Joyce, H. J.; Wong-Leung, J.; Gao, Q.; Tan, H. H.; Jagadish, C. Phase perfection in zinc blende and wurtzite III−V nanowires using basic growth parameters. *Nano Lett.* **2010**, *10*, 908−915.
(41) Lewis, R. B.; Masnadi-Shirazi, M.; Tiedje, T. Growth of high Bi concentration $GaAs_{1-x}Bi_x$ by molecular beam epitaxy. *Appl. Phys. Lett.* **2012**, *101*, No. 082112.
(42) Shu, W.; Zhang, X.; Liu, X.; Huang, H.; Huang, Y.; Ren, X. First-principles investigations of GaAs (112)-(2 × 2) surface reconstruction. *IEEE Advances in Optoelectronics and Micro/nano-optics* **2010**, 11824208.

DOI: 10.1021/acs.nanolett.9b02932
Nano Lett. XXXX, XXX, XXX−XXX

(43) Jacobi, K.; Platen, J.; Setzer, C.; Maárquez, J.; Geelhaar, L.; Meyne, C.; Richter, W.; Kley, A.; Ruggerone, P.; Scheffler, M. Morphology, Surface core-level shifts and surface energy of the faceted GaAs(112)A and (112)B surfaces. *Surf. Sci.* **1999**, *439*, 59−72.
(44) Jenichen, A.; Engler, C. Reconstructions and surface facets of the GaAs(112)A and (112)B surfaces: First-principles DFT supercell calculations. *Surf. Sci.* **2013**, *608*, 204−211.
(45) Steele, J. A.; Lewis, R. A.; Horvat, J.; Nancarrow, M. J. B.; Henini, M.; Fan, D.; Mazur, Y. I.; Schmidbauer, M.; Ware, M. E.; Yu, S.-Q.; Salamo, G. J. Surface effects of vapour-liquid-solid driven Bi surface droplets formed during molecular-beam-epitaxy of GaAsBi. *Sci. Rep.* **2016**, *6*, 28860.

DOI: 10.1021/acs.nanolett.9b02932
Nano Lett. XXXX, XXX, XXX−XXX